JES Focus Issue on Mathematical Modeling of Electrochemical Systems at Multiple Scales in Honor of John Newman

Improving the Lithium Ion Transport in Polymer Electrolytes by Functionalized Ionic-Liquid Additives: Simulations and Modeling

Diddo Diddens,[a,z] Elie Paillard,[a,z] and Andreas Heuer[a,b,z]

[a]*Helmholtz Institute Münster (IEK-12), Ionics in Energy Storage, Forschungszentrum Jülich GmbH, 48149 Münster, Germany*
[b]*Institute of Physical Chemistry, University of Münster, 48149 Münster, Germany*

We present a theoretical study combining molecular dynamics (MD) simulations with an analytical lithium ion transport model [Maitra and Heuer, *Phys. Rev. Lett.* **2007**, 98, 227802] to highlight a novel strategy to increase the lithium mobility in polymer electrolytes based on poly(ethylene oxide) (PEO). This is achieved by using a pyrrolidinium-based ionic liquid (IL) where the cation has been chemically functionalized by a short oligoether side chain [von Zamory et al., *Phys. Chem. Chem. Phys.* **2016**, 18(31), 21539] as an additive. Since the oligoether moieties at the pyrrolidinium cations form pronounced coordinations to the lithium ions for sufficiently long side chains, the ions can be detached from the PEO backbone. In this way, a fundamentally new lithium ion transport mechanism is established (*shuttling mechanism*), in which the lithium dynamics is *decoupled* from the polymer dynamics, the latter typically being slow under experimental conditions. Based on our simulations, we incorporate this novel mechanism into our existing model, which accurately reproduces the observed lithium dynamics. We demonstrate that the use of oligoether-functionalized IL additives significantly increases the lithium diffusivity. Finally, we show that for experimentally relevant electrolytes containing long polymer chains, an even stronger increase of the lithium mobility can be expected.

Manuscript submitted April 10, 2017; revised manuscript received May 11, 2017. Published May 24, 2017. *This paper is part of the JES Focus Issue on Mathematical Modeling of Electrochemical Systems at Multiple Scales in Honor of John Newman.*

Motivation

Solid polymer electrolytes (SPEs) are promising candidates for lithium metal batteries, which are optimal energy storages to power electric vehicles due to their high specific capacity.[1,2] Apart from electromotive applications, high energy densities are also beneficial for portable electronic devices. Typically, SPEs consist of an amorphous polymer matrix, as for instance poly(ethylene oxide) (PEO), and a dissolved lithium salt such as lithium bis(trifluoromethane)sulfonimide (LiTFSI).[3–6] However, the main disadvantage of contemporary SPEs is that, at ambient temperatures, their conductivity is too low for an efficient use in modern energy storages. Consequently, lithium metal batteries typically operate at rather elevated temperatures (70°C–90°C), requiring the stabilization of the temperature (in case of electric vehicles also while being plugged to facilitate fast charging and a quick start of the vehicle).

Apart from other approaches,[7–10] the addition of an ionic liquid (IL) as an additive has been proposed to overcome this deficiency.[11–13] This strategy is mainly motivated by the fact that ILs typically exhibit a wide electrochemical stability window and a low volatility/flammability,[14–16] making them ideal additives for battery electrolytes.

However, despite these efforts, the increase of the lithium diffusivity is still rather modest, as the lithium ions tend to stick to the slow PEO chains despite the larger fraction of anions that can in principle also coordinate to the lithium ions. That is, although Raman measurements indicated an increased coordination between lithium ions and TFSI anions,[12] our previous molecular dynamics (MD) simulations[17,18] of PEO/LiTFSI electrolytes mixed with *N*-methyl-*N*-propyl pyrrolidinium TFSI (Pyr_{13}TFSI) revealed that TFSI coordinates lithium only partially, while the remainder of the lithium coordination sphere is comprised of PEO oxygens. Consequently, virtually all lithium ions remain coordinated to PEO. Thus, rather than a decoupling of lithium ions from the slow polymer chains, the increase of the lithium diffusivity observed experimentally and numerically can be attributed to the plasticizing of the polymer host due to the IL.[17] Since the lithium ions move cooperatively with the PEO segments to which they are attached, also the lithium dynamics[17] is enhanced. Moreover, the IL suppresses the crystallization of PEO at low temperatures, so that the detailed ion transport mechanism remains qualitatively unaffected.[19]

In this work, we use a theoretical approach combining both MD simulations and analytical modeling in order to demonstrate a novel route for increasing the lithium diffusion in polymer electrolytes via IL additives that can facilitate both enhancement mechanisms sketched above, that is plasticizing *and* decoupling of lithium ions from PEO. This is achieved by employing a chemically functionalized IL, in which one of the alkyl substituents (e.g. the propyl substituent in Pyr_{13}) has been replaced by a short oligoether chain comprising m monomers. These *N*-alkoxylether-*N*-methyl pyrrolidinium ILs (denoted as Pyr_{1mEO} in the following, see Figure 1) have recently been introduced as a novel concept to deliberately switch from a TFSI-based lithium coordination to a oligoether-based coordination in experiments.[20] In the present case, the length m of the oligoether side-chain provides a control parameter to tune the decoupling strength (here, we compare $m = 1$ and $m = 4$). By this approach, the

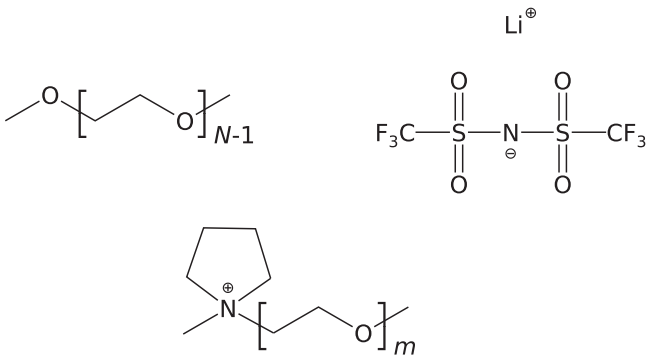

Figure 1. Chemical compounds employed in this study: poly(ethylene oxide) (PEO, upper left) with $N = 64$ monomers, lithium bis(trifluoromethane)sulfonimide (LiTFSI, upper right), and the cation of the IL *N*-alkoxylether-*N*-methyl pyrrolidinium TFSI (Pyr_{1mEO}TFSI, bottom) with $m = 1$ and $m = 4$ monomer(s).

[z]E-mail: d.diddens@fz-juelich.de; e.paillard@fz-juelich.de; andheuer@uni-muenster.de

plasticizing effect is maintained, while at the same time the side chains can detach the lithium ions from the PEO backbone, thus decoupling the lithium dynamics from the polymer dynamics. Once a lithium ion is detached from PEO, it can migrate much faster due to the large center-of-mass mobility of the IL cations as compared to the slow diffusivity of the (typically long) PEO chains. In this way, the IL cations serve as a "shuttle" transporting the lithium ions over larger distances.

Naturally, such a shuttling mechanism can in principle be established by any low-molecular ether additive such as for example glymes, given that the oligoether chain is sufficiently long to form a stable coordination around the lithium ions. In the present article, however, we focus on oligoether-functionalized IL cations, as ILs typically display a low volatility which greatly improves battery safety, especially at elevated temperatures. Moreover, the use of a cationic carrier molecule effectively results in the formation of divalent ions, which might allow one to control the lithium deposition kinetics at lithium metal anodes to a certain degree. Nonetheless, the conclusions of our work can qualitatively be generalized to related additives.

This article is organized as follows: In Theoretical background section, we describe the simulation methodology and our analytical framework, followed by the discussion of the lithium coordination (in particular with respect to its decoupling from PEO) in Lithium coordination section. In Lithium transport mechanism section, we determine the characteristic time scales of the individual transport mechanisms, which are used in Model predictions section for analytical predictions. Finally, in Conclusions section we conclude.

Theoretical Background

MD simulations.—The simulations have been performed with the *Lucretius* code using the APPLE&P polarizable force field.[21–23] Both systems contained 10 methoxy-terminated PEO chains with $N = 64$ monomers each as well as 64 LiTFSI and 128 Pyr_{1mEO}TFSI ion pairs (see also Figure 1), leading to an ether oxygen (EO) to lithium ratio of EO : Li = 10 : 1. For the functionalized IL cation Pyr_{1mEO}, two different side-chain lengths, i.e. $m = 1$ and $m = 4$, have been simulated. The lengths of the cubic simulation boxes were approximately 50 Å and 54 Å, depending on the value of m.

Electrostatic interactions have been treated by the Ewald summation technique with a cutoff radius of 14 Å, an inverse Gaussian charge width of 0.21 $Å^{-1}$, and $8 \times 8 \times 8$ vectors for the part in reciprocal space. Lennard-Jones interactions have been truncated at 14 Å, beyond which a continuum-model dispersion correction was applied. The inducible dipoles were determined iteratively, where dipole-dipole interactions were scaled to zero by a tapering function between 13.5 Å and 14 Å.

The systems were equilibrated in the NpT ensemble at a temperature of $T = 423$ K for about 80 ns using a reduced cutoff radius of 10 Å and $3 \times 3 \times 3$ reciprocal vectors for the Ewald summation, followed by equilibration runs of roughly 10 ns with the ordinary cutoff radius and number of reciprocal vectors (see above). Subsequently, production runs of 30 ns ($m = 1$) and 20 ns ($m = 4$) have been performed in the NpT ensemble at 423 K. The temperature and pressure were maintained by a Nosé-Hoover chain thermostat[24] with a coupling frequency of 0.01 fs^{-1} and a barostat with coupling frequency of 0.0005 fs^{-1}. Periodic boundary conditions were applied in all three dimensions. All bonds were constrained by the SHAKE algorithm.[25,26] A multiple-time-step integration scheme[27,28] was used to integrate the equations of motion, where a time step of 0.5 fs has been used for bonds and angles. For torsions and nonbonded interactions up to a distance of 7 Å, a time step of 1.5 fs was used, and finally, for nonbonded interactions between atoms separated more than 7 Å, a time step of 3 fs was used.

Analytical model.—To rationalize our findings from the MD simulations, we employ an analytical lithium ion transport model,[29] which has already been successfully applied to ternary polymer electrolytes of the type PEO/LiTFSI/Pyr_{13}TFSI.[17,18] This model is based on both the Rouse model[30,31] (taking into account the contribution of the polymer dynamics) and the Dynamic Bond Percolation (DBP) model[32] (accounting for random ion hopping processes within the polymer matrix). In particular, three different microscopic transport mechanisms typically found for PEO-based polymer electrolytes[29,33–35] are taken into account, of which one mechanism is composed of two subcontributions. To assess their individual impact on the overall lithium dynamics, each mechanism is quantified by a characteristic time scale (see also sketch in Figure 2): First, the lithium ions diffuse along the backbone of the coordinating PEO chains. The time scale required to explore the entire chain is denoted as τ_1. Second, the PEO chains themselves also display significant motion above their glass transition temperature, transporting the coordinating lithium ions in this way. For sufficiently short polymers, this motion consists of the center-of-mass motion and the segmental dynamics of the chains, the former becoming irrelevant in the limit of long chains. The segmental motion is quantified by a relaxation time τ_2, which can be identified as an effective Rouse time, known from polymer physics.[31] Third, a lithium ion coordinating to a given PEO chain can be transferred to another chain. The average residence time at a given chain is denoted as τ_3. Note that the last mechanism can be viewed as a renewal event within the framework of the DBP model,[32] after which the lithium dynamics becomes uncorrelated to its past.

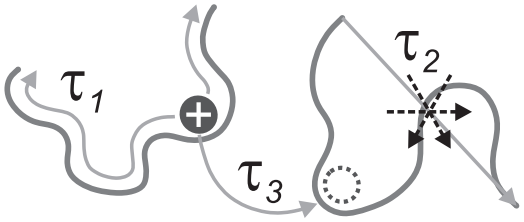

Figure 2. Sketch of the microscopic lithium transport mechanisms taken into account by the analytical model.[29] Each mechanism is quantified by a characteristic time scale.

In case of the decoupling of lithium ions from the PEO chains, a fourth mechanism emerges, in which the ion diffuses cooperatively with a few IL molecules (that is IL anions and/or IL cations). However, since the ion dynamics becomes statistically uncorrelated after being transferred from PEO to IL molecules or vice versa, a correction can be estimated in a straightforward manner. In particular, the original and purely PEO-based lithium diffusivity D_{Li}^{PEO} simply has to be substituted by $D_{Li} = (1 - p_{IL})\, D_{Li}^{PEO} + p_{IL}\, D_{IL}$, where p_{IL} denotes the equilibrium fraction of lithium ions moving cooperatively with the coordinating IL molecules, and D_{IL} is the diffusivity of these ions during that time. Note that on this level of description, the diffusivity is independent of the time scale during which the individual lithium ions are decoupled from the PEO chains.

Lithium Coordination

In classical PEO-based SPEs, the lithium ions are typically coordinated by 4–6 EOs of the PEO backbone, where the latter wraps helically around the ion.[29,34,35] Alternatively, the lithium ions can also be partly or entirely coordinated to the respective anions of the lithium salt, depending on the salt's tendency to form ion pairs or ion clusters, which in turn affects the lithium dynamics[36] (with TFSI being a weakly coordinating anion, as also reflected by our previous simulations[35]). Due to the choice of the conventional pyrrolidinium ion with alkyl substituents in the ternary SPEs investigated so far experimentally[14–16] and numerically,[17,18] the IL cation is essentially non-coordinating.

In the present case, however, the EOs from the side chain of Pyr_{1mEO} can also coordinate to the lithium ions, and possibly even decouple them from the PEO chains as motivated above. Therefore, we investigate the lithium coordination structure in a first step. From the radial distribution functions (RDFs) between lithium ions and the EOs of the PEO backbone (see Figure S1 in the Supplementary Material),

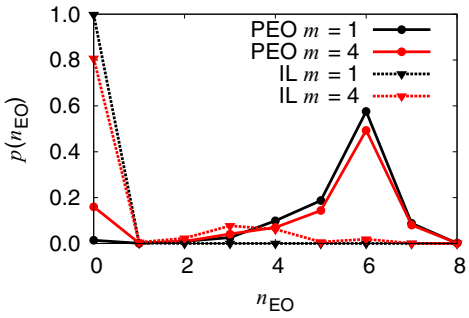

Figure 3. Probability distribution functions that a given lithium ion is coordinated to n_{EO} ether oxygen atoms of PEO (solid lines) and IL cations (i.e. Pyr_{1mEO}, dashed curves) for $m = 1$ and $m = 4$.

we observe a strong first peak that is only weakly dependent on m, indicating that in both systems, significant coordinations between the lithium ions and PEO are present. Also the respective RDFs between lithium and the EOs from the Pyr_{1mEO} side chains show a first coordination peak (Figure S1). However, a closer inspection reveals that this peak is mainly visible for $m = 4$, indicating a pronounced coordination, while it is very small for $m = 1$, showing that for the latter, the coordination is essentially unstable. The RDFs between lithium ions and oxygen atoms from TFSI also show a distinct first peak, which is slightly larger for $m = 4$, likely due to the larger molecular volume of the IL cation giving rise to a slightly different normalization factor of the two RDFs. In the following, we define a given Li^+-EO pair to be coordinated if their mutual distance is less than 3.5 Å, i.e. the distance for which the minimum after the first coordination peak is observed for all lithium-EO RDFs. Similarly, we define a lithium ion and a TFSI molecule to be bound if their distance is not larger than 3.0 Å.

Figure 3 shows the probability distribution functions that a given lithium ion is coordinated to n_{EO} EOs, either from the PEO backbone (solid lines) or the Pyr_{1mEO} cations (dashed lines). The PEO curves display a maximum centered around the typical coordination number of $n_{EO} = 6$. Interestingly, while the probability $p_{IL} = p(n_{EO} = 0)$ is marginal for $m = 1$, a significant fraction of lithium ions entirely detached from PEO can be observed for $m = 4$ (see also detailed p_{IL}-values in Table I). This indicates that for the former, the side chain is too short to form stable coordinations. However, we observe a minor lithium decoupling due to the formation of short-lived coordinations involving 2–3 TFSI anions rather than IL cations (note that only about 0.2% of all lithium ions are coordinated to EOs from Pyr_{1mEO} for $m = 1$). In contrast, stable coordinations between lithium and IL cations and thus successful lithium decoupling can be observed for $m = 4$. In total, the vast majority (99%) of PEO-coordinated lithium ions binds to a single PEO chain only, which differs from the results of our previous study,[17] where significant amounts of ions coordinating to two PEO chains were found. This difference can essentially be related to the different EO : Li ratio (EO : Li = 20 : 1 in Ref. 17) resulting in fewer free EOs required to bridge two chains, as well as the stronger dilution of PEO in the present study, which both favors locally compact coordination shells at a single chain. Finally, about 25% ($m = 1$) and 30% ($m = 4$) of all lithium ions are at least partly coordinated by TFSI anions, either when being decoupled or attached to PEO. This observation can again be rationalized by the relatively low EO : Li ratio, as the limited number of coordinating EOs is compensated by enhanced TFSI coordinations despite being a weakly coordinating anion. Due to the evident decoupling for $m = 4$, significant dynamical contributions of these ions to the overall lithium diffusion coefficient can be expected, requiring an adaption of the transport model, as discussed in Model predictions section.

Lithium Transport Mechanism

Intersegmental transfer.—We start our analysis with the determination of the mean residence time that a given lithium ion remains coordinated to a given PEO chain, denoted as τ_3. It has to be mentioned within this context that in the experimentally relevant long-chain limit ($N \to \infty$), the transition of lithium ions between different chains or their decoupling from the latter is vital for the macroscopic long-range transport, as the center-of-mass diffusion becomes negligible in this case. Therefore, these events can be considered as renewal events within the framework of the DBP model,[32] as the dynamics before and after such a transfer is uncorrelated,[29] and the lithium ions can migrate over macroscopic distances in this way.

In case that all lithium ions are coordinated to PEO chains, the average residence time can be estimated by the rate τ_3^{-1} of ion transfers between two distinct PEO chains,[29]

$$\frac{1}{\tau_3} = \frac{N_{trans}}{t_{sim}\, N_{Li^+}}, \qquad [1]$$

where N_{trans} denotes the number of these transfer events, t_{sim} the total simulated time, and N_{Li^+} the number of lithium ions in the simulation box. However, due to the fact that a certain fraction of lithium ions is coordinated by IL molecules only (in particular for $m = 4$), one has to use a corrected expression instead:

$$\frac{1}{\tau_3} = \frac{N_{trans}^{PEO}}{(1 - p_{IL})\, t_{sim}\, N_{Li^+}} \qquad [2]$$

Here, the reduced or effective time $(1 - p_{IL})\, t_{sim}$ accounts for the fact that not all ions are coordinated to PEO (given by p_{IL}, see Table I), and N_{trans}^{PEO} contains only those transfer events in which a lithium ion is detached from PEO, irrespective if it is transferred to another chain or IL molecules. The resulting values are listed in Table I. We observe that τ_3 is about 20% shorter for $m = 4$ than for $m = 1$ due to the enhanced decoupling of lithium ions by Pyr_{1mEO} ions, resulting in both a slightly larger number of free PEO segments required to receive an ion as well as an increased decoupling frequency. It is worth noting that the τ_3-values are significantly larger than in our previous study[17] ($\tau_3 \approx 17 - 24$ ns), which can be understood by the lower fraction of free EOs (required to receive a lithium ion) for a ratio of EO : Li = 10 : 1 (as opposed to EO : Li = 20 : 1 in Ref. 17). In addition, the PEO volume fraction is slightly lower by about 15–30% for the present systems, rendering the encounter of two PEO segments necessary for a transfer less likely.

Motion along the backbone.—Next, we characterize the diffusion of the lithium ions along the polymer chains. As time evolves, a coordinating monomer may detach from the lithium ion, whereas another monomer from the other end of the coordinating PEO strand (typically 4–6 monomers, see Figure 3) attaches to the ion. In this way, the lithium ion performs a random-walk-like motion along the polymer backbone. In order to quantify this motion, we define the average monomer index n of the coordinating PEO strand as an effective coordinate. The mean squared displacement (MSD) $\langle \Delta n^2(t) \rangle$ along

Table I. Structural parameters p_{IL} and $\langle R_g^2 \rangle$, time scales τ_1, τ_2 and τ_3 defined by the transport model, mean lifetime of pure lithium-IL complexes τ_{IL}, and various diffusion coefficients as extracted from the simulation data or calculated by the transport model (see text for further explanation).

m	p_{IL} [%]	$\langle R_g^2 \rangle$ [Å^2]	τ_1 [ns]	τ_R [ns]	τ_2 [ns]	τ_3 [ns]	τ_{IL} [ns]	D_{PEO} [Å^2/ns]	D_{IL} [Å^2/ns]	$D_{Li}(N = 64)$ [Å^2/ns]	$D_{Li}(N \to \infty)$ [Å^2/ns]
1	1.4	239	481	49	53	96	3	2.5	13.4	3.3	1.1
4	16.0	240	455	39	48	78	17	2.8	11.6	4.9	2.8

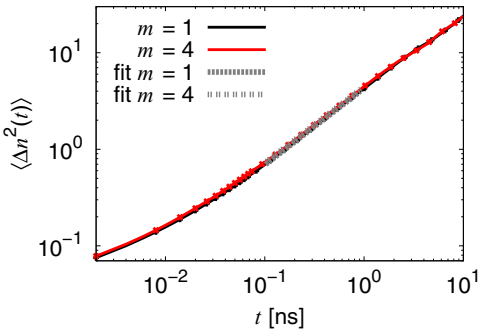

Figure 4. Mean squared change $\langle \Delta n^2(t) \rangle$ of the average monomer index n of the PEO strand coordinating to a given lithium ion as a function of time t. The dashed curves indicate the functions $\langle \Delta n^2(t) \rangle = c\, t^{\alpha}$ that have been fitted to the data in the range from 0.1–1 ns.

this coordinate is shown in Figure 4. Based on this definition, the diffusion coefficient D_1 related to the diffusion along this effective coordinate can in principle be computed from the MSD by the Einstein relation

$$D_1 = \lim_{t \to \infty} \frac{\langle \Delta n^2(t) \rangle}{2\, t}. \qquad [3]$$

Subsequently, τ_1 can be obtained from the transport model via [29]

$$\tau_1 = \frac{(N-1)^2}{D_1\, \pi^2}, \qquad [4]$$

with $N - 1$ being the largest accessible distance for which the entire polymer chain has been explored by the ion.

From Figure 4 we observe that the motion along the backbone is still subdiffusive with a dependence of roughly $\langle \Delta n^2(t) \rangle \propto t^{0.8}$ throughout the entire accessible time scale, making the direct estimation of D_1 impossible. Therefore, one would ideally determine D_1 at $t = \tau_3$ to capture the total number of PEO monomers a given lithium ion has traveled while being coordinated to a particular chain. Unfortunately, this time scale exceeds the length of our simulations, which is why we extrapolated the scaling $\langle \Delta n^2(t) \rangle \propto t^{0.8}$ observed in Figure 4 to $t = \tau_3$ in order to estimate $D_1(t = \tau_3)$ and, correspondingly, τ_1 (Table I). We deem the error related to the extrapolation to be minor, as a comparative (and just as approximative) determination of the D_1 at $t \approx 5$ ns, related to the upper time range in Figure 4, yields values of $\tau_1 = 288$ ns for $m = 1$ and $\tau_1 = 286$ ns for $m = 4$. Despite the large deviation from the respective values in Table I, τ_1 is still significantly larger than τ_2 (see below) and τ_3 for both m-values, so that the quantitative impact of this mechanism on the overall lithium dynamics is marginal for either fitting scheme.

In total, we observe only a minor effect of m on τ_1 (Table I). The slightly lower value for $m = 4$ can essentially be attributed to the implicit dependence of τ_1 on τ_3 due to the extrapolation. Consistently, $\langle \Delta n^2(t) \rangle$ is basically identical for both m. Compared with the electrolytes from our previous publications[17,18,35] with EO : Li = 20 : 1 ($\tau_1 \approx$ 130–150 ns), this mechanism is significantly hampered due to the reduced number of free monomers and the associated crowding of the PEO chains by lithium ions. Similar issues have also been discussed in Ref. 18, where larger τ_1-values have been found if the EO : Li ratio is lowered (here, values of up to $\tau_1 \approx 300$ ns have been found for EO : Li = 8 : 1 and $N = 54$, thus roughly falling into the same range as the values in Table I).

Cooperative dynamics with the polymer chains.—Finally, we study the cooperative motion of the lithium ions with the polymer segments. To this end, we compute the MSD $\langle \Delta \mathbf{R}^2_{\mathrm{EO}}(t) \rangle$ of the EOs of PEO and of the respective attached lithium ions in the center-of-mass frame of the polymer chains (Figure 5). For the PEO monomers, we distinguish between average monomers (black solid lines) and monomers bound to lithium ions (black dashed lines). In the latter

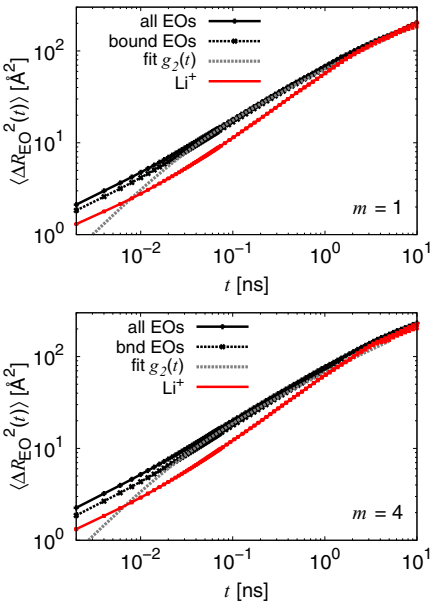

Figure 5. Mean squared displacement $\langle \Delta \mathbf{R}^2_{\mathrm{EO}}(t) \rangle$ of the ether oxygens of PEO (relative to the center of mass of the chains) as a function of time t for (a) $m = 1$ and (b) $m = 4$. A distinction has been made between average monomers (black solid lines), monomers bound to a lithium ion (black dashed lines), and the respective attached ions (red solid line). The gray dashed curves show the Rouse fits (Equation 5) for the bound PEO monomers that have been applied in the range of 0.1–0.6 ns. The respective fits for the average ether oxygens (not shown) have been applied in the range of 0.1–1 ns.

case, only observations in which the monomer was bound to the same ion throughout the entire observation time t have been considered, the same condition has been applied for the computation of the MSD of the attached lithium ions (red lines). For both m, we observe a subdiffusive Rouse-like motion of the PEO monomers irrespective of their coordination type (that is bound to a lithium ion or not). The dynamics of the attached lithium ions is slower than that of the EOs on short time scales (up to about 1 ns), which can be rationalized by the fact that the latter experience additional dynamical contributions due to the internal degrees of freedom of the PEO backbone. On larger time scales, however, the motion of the ions becomes comparable to that of the coordinating EOs. For this reason, the Rouse-type motion of the bound PEO segments can also be utilized to quantify the dynamics of the attached lithium ions.

To extract the corresponding time scale τ_2, the Rouse expression for the segmental MSD,

$$g_2(t) = \frac{12 \langle R_g^2 \rangle}{\pi^2} \sum_{p=1}^{N-1} \frac{\left[1 - \exp\left(-\frac{t\, p^2}{\tau_2}\right)\right]}{p^2}, \qquad [5]$$

has been fitted to the data (dashed gray curves in Figure 5). Here, $\langle R_g^2 \rangle$ is the mean squared radius of gyration of the polymer chains characterizing their average coil size, which was extracted from the numerical data (see Table I). Interestingly, the ratios of the mean squared end-to-end vector and $\langle R_g^2 \rangle$ are close to six, indicating that the chain structure is approximately Gaussian despite the pronounced coordination of lithium ions to the chains or the presence of the IL, thus additionally validating our analysis in terms of the Rouse model.

We applied the fit, given by Equation 5, to both the MSD of the average EOs, yielding the global polymer relaxation time or Rouse time τ_R, and to the MSD of the bound monomers, resulting in the effective Rouse time τ_2 relevant for the lithium motion. The latter fit curves are shown as gray dashed lines in Figure 5, the corresponding values for τ_R and τ_2 are shown in Table I. As can be seen from Figure 5, the fits agree quantitatively from a few hundred picoseconds on. On shorter time scales, the MSD of the segments is mainly governed

by the chemical details of the backbone, which is not captured by the simplistic Rouse model. We observe that both τ_R and τ_2 are smaller by respective amounts of about 20% and 10% for $m = 4$ than for $m = 1$. This can be interpreted as an effect of the larger number of free PEO segments, as also reflected by the larger decrease for τ_R than for τ_2. In total, the τ_2-values are comparable to those of our previous study[17] ($\tau_2 = 68$ ns for the largest IL fraction, EO : Li = 20 : 1, and $N = 54$) despite the larger chain length and the reduced number of free PEO segments in the present study, as the IL amount per PEO monomer exceeds the values of the previous compositions. Therefore, although the PEO chains are rather crowded, the accompanying slowdown can apparently be overcompensated by the addition of sufficiently large fractions of IL (see also discussion in Ref. 18). Consequently, we observe a net plasticizing, which is also reflected by the fact that $\tau_2 \ll \tau_1$ (Table I).

Of course, in the limit of short chains, the center-of-mass diffusion of the PEO chains significantly contributes to the overall polymer dynamics, and thus also to the diffusion of the attached lithium ions. The respective diffusion coefficients D_{PEO} for the PEO chains are given in Table I. Since the center-of-mass motion is uncorrelated to the internal segmental dynamics to a good approximation, its contribution to the lithium diffusion can simply be modeled as an additive term (although this assumption is not strictly fulfilled for polymer melts[37,38]).

Model Predictions

Reproduction of the lithium dynamics.—Before applying our transport model to the limit of long chains ($N \to \infty$), which are typically employed in experiments, we reproduce the empirically observed lithium MSD in a first step (denoted as g_{Li}) in a first step. Since the lithium motion at the PEO chains is uncorrelated to the motion in the IL-rich regions due to the renewal property of the transfer processes,[29,32] the lithium ion dynamics can effectively be modeled as a random walk with a random change in direction after each transfer process.[35] Between two subsequent transfer processes separated by the waiting time $\tilde{t}$, the mean squared step length of this random walk is given by a Rouse-like expression of the type

$$g_{12}(\tilde{t}) = \frac{12\langle R_g^2\rangle}{\pi^2}\sum_{p=1}^{N-1}\frac{\left[1-\exp\left(-\frac{\tilde{t}\,p^2}{\tau_{12}}\right)\right]}{p^2}, \qquad [6]$$

which is characterized by a combined relaxation rate $\tau_{12}^{-1} = \tau_1^{-1} + \tau_2^{-1}$ due to both the diffusion along the backbone and the segmental motion[29] (in contrast to g_2 in Equation 5, which only contains the polymer contribution). In the following, we assume that the distribution function $p(\tilde{t})$ of the individual residence times $\tilde{t}$ is exponential,[29,35] allowing us to calculate both the probability that k transfer processes have occurred during observation time t and the respective $\tilde{t}$-values. By averaging over all k-values with a reasonably high probability and a large number of independent random walks, we obtain the lithium MSD $\langle\Delta\mathbf{R}_{RW}^2(t)\rangle$ arising from all three PEO-based transport mechanisms. As an alternative to this numerical average, an analytical expression can be obtained by integrating Equation 6 over the exponentially distributed waiting times, i.e. $\langle g_{12}(\tau_3)\rangle = (1/\tau_3)\int_0^\infty d\tilde{t}\exp(-\tilde{t}/\tau_3)\,g_{12}(\tilde{t})$, leading to

$$\langle g_{12}(\tau_3)\rangle = \frac{12\langle R_g^2\rangle}{\pi^2}\sum_{p=1}^{N-1}\frac{1}{p^2}\left[1-\frac{1}{p^2\frac{\tau_3}{\tau_{12}}+1}\right]. \qquad [7]$$

Here, the brackets $\langle\ldots\rangle$ of $\langle g_{12}(\tau_3)\rangle$ indicate the average over all possible residence times, which depends on the mean τ_3 (see Ref. 29 for further details).

The two remaining contributions arise from the center-of-mass motion of the PEO chains and the free diffusion of lithium ions not bound to PEO. As discussed above, the center-of-mass motion of PEO is independent from the internal polymer dynamics, thus simply constituting an additive contribution characterized by D_{PEO}, which can easily be determined from the simulation data (Table I and Figure S2 in the Supplementary Material). In principle, the same approach can be applied to capture the effect of the free lithium ions, however, it has to be assured that the ions remain decoupled sufficiently long to become diffusive. In analogy to Equation 2, we define $\tau_{IL}^{-1} = N_{trans}^{IL}/(p_{IL}t_{sim}N_{Li^+})$ as the average time during which a lithium ion is solely coordinated by IL cations or TFSI anions. The resulting values are reported in Table I. Consistent with the static probability p_{IL}, the average residence time in the IL-rich regions is rather short for $m = 1$ (TFSI coordinations only), while τ_{IL} is significantly larger for $m = 4$ (coordinations by Pyr_{1mEO} and TFSI). Nonetheless, for both m, the IL-coordinated lithium ions become diffusive from roughly 1 ns on (see Figure S2 in the Supplementary Material), which is shorter than the τ_{IL} in Table I. Therefore, we define D_{IL} as an effective diffusion coefficient of the lithium ions detached from PEO (Table I).

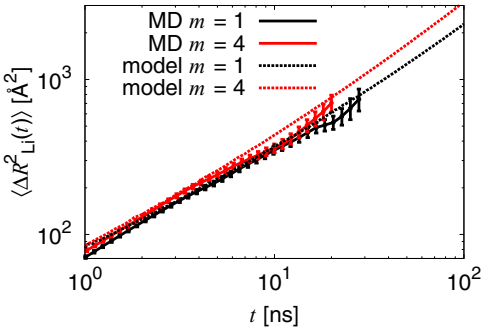

Figure 6. Lithium mean squared displacement $\langle\Delta\mathbf{R}_{Li}^2(t)\rangle$ as extracted from the simulations (solid lines) and the predictions of the lithium transport model $g_{Li}(t)$ (dashed curves) as a function of time t for $m = 1$ and $m = 4$.

Since both types of motion discussed above are uncorrelated to the dynamics due to the three transport mechanisms, we finally arrive at

$$g_{Li}(t) = (1-p_{IL})\left[\langle\Delta\mathbf{R}_{RW}^2(t)\rangle + 6D_{PEO}t\right] + p_{IL}\,6D_{IL}t. \qquad [8]$$

The resulting curves are shown in Figure 6 together with the lithium MSD $\langle\Delta\mathbf{R}_{Li}^2(t)\rangle$ extracted from the simulation data. We observe that on time scales of up to about 10 ns, both model curves agree reasonably well with the actually observed lithium MSDs. On larger time scales, however, the statistics of the simulation curves deteriorates. Nonetheless, the model allows us to estimate the diffusion coefficients D_{Li} from the diffusive regime starting from a few ten nanoseconds on (Table I).

When comparing D_{Li} for $m = 1$ and $m = 4$, one notices that the latter is larger by as much as 50%, reflecting the decoupling by the IL cation with the longer alkoxylether chain. On short time scales, however, the lithium ions are only marginally faster for $m = 4$, as most lithium ions (that is 84%) are still coordinated to their initial PEO chain, and did not yet undergo a transfer process. Although the remaining fraction of free lithium ions displays diffusive motion from approximately 1 ns on, the ions coordinated to PEO move faster for short t due to the internal degrees of freedom of the polymer chains despite being subdiffusive. Thus, in the short-time regime, the dynamical impact of the former is rather minute. Contrarily, in the long-time limit, the relative contribution of the IL-based transport to the overall D_{Li}-value is as large as 38% for $m = 4$, while it is only about 6% for $m = 1$. As discussed in Lithium coordination section, the IL cation with a single EO only is not capable to detach the lithium ions from the PEO chains. The remaining increase of D_{Li} for $m = 4$ as compared to $m = 1$ can be attributed to the slightly smaller values for τ_2 and τ_3, as well as the slightly larger center-of-mass diffusion (Table I). Of course, for short chains, the center-of-mass contribution of PEO is dominating the overall MSD (relative contributions of 74% for $m = 1$ and 48% for $m = 4$).

Implications for experiments.—Finally, we use the transport model to compute D_{Li} in the experimentally relevant long-chain limit (i.e. $N \to \infty$) by relying on simple scaling arguments from poly-

mer theory.[31] In particular, from Equation 4, one has $\tau_1 \propto N^2$, and from the Rouse model, one expects the same scaling for τ_2, that is $\tau_2 \propto N^2$.[31] Finally, since the transfer processes only involve two local PEO segments, one has $\tau_3 \propto N^0$.

Of course, for the scaling of τ_2, entanglement effects may in principle become relevant, leading to a stronger dependence of the segmental relaxation time on N.[31] However, if τ_3 is shorter than the entanglement time τ_e, i.e. the time scale from which the chains experience the tube constraint and perform reptation dynamics, entanglement effects are irrelevant for the lithium motion. From experiments, one finds values between 75 monomers[39] and 225 monomers[40] for the entanglement length N_e of PEO, leading to estimated $\tau_e = \tau_R(N_e)$ of 60–550 ns based on the τ_R-values in Table I. Thus, according to these estimates, τ_3 and τ_e might in principle fall into the same range. However, one additionally has to keep in mind that the above considerations are valid for pure PEO melts, whereas in the present case, the melt is diluted by IL and lithium salt. When reducing the volume concentration c of the PEO monomers, one expects an increase of the entanglement length as $N_e' = N_e\, c^{-2}$, and, consequently, $\tau_e' = \tau_e\, c^{-4}$.[41] For $m = 1$, the monomer volume fraction is only 38% of the respective value of pure PEO,[18] for $m = 4$ it is reduced even stronger down to 30% of the original volume fraction. As a consequence, the τ_e' increase by respective factors of about 50 and 120 as compared to the bare τ_e. This steep dependence clearly demonstrates that entanglement effects can safely be ignored for the electrolytes investigated in the present study.

In analogy to Equation 8, we define the overall diffusion constant as

$$D_{Li} = (1 - p_{IL})\, \frac{\langle g_{12}(\tau_3)\rangle}{6\,\tau_3} + p_{IL}\, D_{IL}, \qquad [9]$$

where $\langle g_{12}(\tau_3)\rangle$ is the residence-time-averaged MSD the lithium ions bound to PEO experience (Equation 7). As before, for D_{IL} the values in Table I have been used. For the sake of simplicity, we assume that D_{IL} is independent of N. Corrections to this approximation can in principle be incorporated into the model, but do not alter our conclusions quantitatively or provide any new insights (rather, further computationally expensive large-scale simulations would be required).

The predicted D_{Li}-values for $N \to \infty$ are summarized in Table I. Here, the increase of D_{Li} for $m = 4$ when compared to $m = 1$ (factor of 2.5) is much more pronounced than for $N = 64$ despite lower absolute values resulting from the vanishing center-of-mass motion of PEO. While the relative dynamical contribution of decoupled lithium ions is minor for $m = 1$ (16%), it constitutes the main part for $m = 4$ (66%). In total, these findings demonstrate that the use of alkoxylether-functionalized ILs as additives in SPEs indeed increases the lithium mobility significantly for sufficiently large m. This effect becomes especially pronounced in the limit of long or crosslinked chains, for which the contribution of D_{PEO} is negligible. For these reasons, we expect that the use of an ether-functionalized IL with a sufficiently long side chain will clearly improve the performance of SPEs in experiments.

Conclusions

In this article, we presented a theoretical study combining MD simulations with an analytical lithium ion transport model[29] in order to point out a new approach to increase the lithium diffusivity in ternary polymer electrolytes. This is achieved by a using a chemically functionalized IL, in which the pyrrolidinium cation bears a short oligoether substituent,[20] which for a sufficient number of monomers can coordinate to the lithium ions and even detach them from the PEO backbones. In this way, a novel lithium transport mechanism is introduced (coined as *shuttling mechanism*), as the lithium ions become dynamically *decoupled* from the slow polymer chains. This contrasts the microscopic transport mechanism in conventional SPEs, where all ion transport processes occur at the PEO chains.

It turned out that for a side-chain length of $m = 1$ monomer, no stable coordination between lithium ions and the IL cation can be established, while for $m = 4$, about 16% of the lithium ions were decoupled from PEO. In a first step, the PEO-based transport mechanisms were quantified by our previously developed model.[29] In particular, the lithium motion along the PEO backbone is essentially negligible due to the low ratio of ether monomers and lithium ions, leading to the crowding of the PEO chains that hinders the ions to diffuse along the backbone. Contrarily, the IL plasticizes the PEO matrix, as the segmental relaxation of the polymers takes place on substantially shorter time scales (see also our previous work[17]). In total, we observed only minor effects of the side-chain length of the IL cations on these two intramolecular mechanisms based on PEO.

The main impact of the IL on the lithium dynamics stems from the dynamical decoupling of the lithium ions from the PEO chains. In addition to the ordinary lithium transitions between two PEO chains observed previously,[17,35] a significant amount of lithium ions migrates through the electrolyte while being only coordinated by IL cations and anions for $m = 4$ in the present case. Since the typical residence time in the IL-rich regions is on the order of a few ten nanoseconds, the dynamical contribution of these ions can readily be incorporated into our transport model via an additive correction term based on the effective diffusion coefficient of the respective ions. In total, the relative contribution of these free ions to the overall lithium diffusion coefficient is 38% for the numerically investigated PEO chain length of $N = 64$ monomers, while it becomes even larger in the experimentally relevant long-chain limit (66%). In the latter regime, the lithium diffusivity is even 2.5 times larger when using pyrrolidinium cations with four ether monomers than for essentially non-coordinating pyrrolidinium ions with a single monomer only. For these reasons, the use of chemically functionalized ILs indeed seems to be a fruitful approach to overcome the current limitations of SPEs.

Finally, one may wonder about appropriate lengths of the side chain, i.e. the proper choice of m in experiments. In particular, the impact on the lithium diffusivity is expected to be optimum if, on one hand, the diffusion constant D_{IL} is still sufficiently close to that of the bare IL, and, on the other hand, the decoupling expressed by p_{IL} is as large as possible. The latter aspect suggests the use of even larger oligoether substituents. Since for $m = 4$ the diffusion constant D_{IL} is only slightly reduced as compared to $m = 1$, one may indeed expect that the optimal value is significantly larger than 4. An experimental study, using different values of m together with further simulations, is already underway. In general terms, we would like to stress that molecular dynamics simulations may both rationalize and predict transport properties of electrolytes. This type of information may serve as an essential input in the modeling of batteries, as pioneered by Newman already a long time ago.[42–44]

Acknowledgments

The authors thank the federal state NRW for funding via the program Az. 433 "Ion Conductors for Highly Efficient Energy Storages" and the German Research Foundation (Deutsche Forschungsgemeinschaft, DFG) through the research unit "Nonlinear Response to Probe Vitrification" (FOR 1394) and grant DI 1959/2-1 (DD).

References

1. K. Xu, *Chem. Rev.*, **104**, 4303 (2004).
2. Z. Li, J. Huang, B. Y. Liaw, V. Metzler, and J. Zhang, *J. Power Sources*, **254**, 168 (2014).
3. F. M. Gray, *Solid Polymer Electrolytes* (VCH New York etc., 1991).
4. D. Fenton, J. Parker, and P. Wright, *Polymer*, **14**, 589 (1973).
5. M. B. Armand, *Annu. Rev. Mater. Sci.*, **16**, 245 (1986).
6. P. Bruce and C. Vincent, *J. Chem. Soc., Faraday Trans.*, **89**, 3187 (1993).
7. W. Gang, J. Roos, D. Brinkmann, F. Capuano, F. Croce, and B. Scrosati, *Solid State Ionics*, **53**, 1102 (1992).
8. M. Borghini, M. Mastragostino, and A. Zanelli, *Electrochim. Acta*, **41**, 2369 (1996).
9. L. Bandara, M. Dissanayake, and B.-E. Mellander, *Electrochim. Acta*, **43**, 1447 (1998).
10. Y.-T. Kim and E. S. Smotkin, *Solid State Ionics*, **149**, 29 (2002).
11. J.-H. Shin, W. A. Henderson, and S. Passerini, *Electrochem. Commun.*, **5**, 1016 (2003).

12. M. Joost, M. Kunze, S. Jeong, M. Schönhoff, M. Winter, and S. Passerini, *Electrochim. Acta*, **86**, 330 (2012).
13. I. Osada, J. von Zamory, E. Paillard, and S. Passerini, *J. Power Sources*, **271**, 334 (2014).
14. Y. Huo, S. Xia, S. Yi, and P. Ma, *Fluid Phase Equilib.*, **276**, 46 (2009).
15. L. Larush, V. Borgel, E. Markevich, O. Haik, E. Zinigrad, D. Aurbach, G. Semrau, and M. Schmidt, *J. Power Sources*, **189**, 217 (2009).
16. W. Xu, L.-M. Wang, R. A. Nieman, and C. A. Angell, *J. Phys. Chem. B*, **107**, 11749 (2003).
17. D. Diddens and A. Heuer, *ACS Macro Lett.*, **2**, 322 (2013).
18. D. Diddens and A. Heuer, *J. Phys. Chem. B*, **118**, 1113 (2014).
19. J. Chattoraj, D. Diddens, and A. Heuer, *J. Chem. Phys.*, **140**, 024906 (2014).
20. J. von Zamory, G. A. Giffin, S. Jeremias, F. Castiglione, A. Mele, E. Paillard, and S. Passerini, *Phys. Chem. Chem. Phys.*, **18**, 21539 (2016).
21. O. Borodin and G. D. Smith, *J. Phys. Chem. B*, **110**, 6279 (2006).
22. O. Borodin and G. D. Smith, *J. Phys. Chem. B*, **110**, 6293 (2006).
23. O. Borodin, *J. Phys. Chem. B*, **113**, 11463 (2009).
24. G. J. Martyna, M. L. Klein, and M. Tuckerman, *J. Chem. Phys.*, **97**, 2635 (1992).
25. J.-P. Ryckaert, G. Ciccotti, and H. J. Berendsen, *J. Comput. Phys.*, **23**, 327 (1977).
26. B. J. Palmer, *J. Comput. Phys.*, **104**, 470 (1993).
27. G. J. Martyna, D. J. Tobias, and M. L. Klein, *J. Chem. Phys.*, **101**, 4177 (1994).
28. G. J. Martyna, M. E. Tuckerman, D. J. Tobias, and M. L. Klein, *Mol. Phys.*, **87**, 1117 (1996).
29. A. Maitra and A. Heuer, *Phys. Rev. Lett.*, **98**, 227802 (2007).
30. P. E. Rouse Jr., *J. Chem. Phys.*, **21**, 1272 (1953).
31. M. Doi and S. F. Edwards, *The Theory of Polymer Dynamics*, Vol. 73 (oxford university press, 1988).
32. A. Nitzan and M. A. Ratner, *J. Phys. Chem.*, **98**, 1765 (1994).
33. F. Müller-Plathe and W. F. van Gunsteren, *J. Chem. Phys.*, **103**, 4745 (1995).
34. O. Borodin and G. D. Smith, *Macromolecules*, **39**, 1620 (2006).
35. D. Diddens, A. Heuer, and O. Borodin, *Macromolecules*, **43**, 2028 (2010).
36. A. Maitra and A. Heuer, *J. Phys. Chem. B*, **112**, 9641 (2008).
37. J. Farago, H. Meyer, and A. Semenov, *Phys. Rev. Lett.*, **107**, 178301 (2011).
38. J. Farago, H. Meyer, J. Baschnagel, and A. Semenov, *J. Phys.: Condens Matter*, **24**, 284105 (2012).
39. J. Shi and C. A. Vincent, *Solid State Ionics*, **60**, 11 (1993).
40. M. Appel and G. Fleischer, *Macromolecules*, **26**, 5520 (1993).
41. T. A. Kavassalis and J. Noolandi, *Macromolecules*, **22**, 2709 (1989).
42. M. Doyle and J. Newman, *Electrochim. Acta*, **40**, 2191 (1995).
43. K. E. Thomas, J. Newman, and R. M. Darling, in *Advances in Lithium-ion Batteries* (Springer, 2002) pp. 345–392.
44. J. Newman and K. E. Thomas-Alyea, *Electrochemical Systems* (John Wiley & Sons, 2012).